Journal of Materials Chemistry C

PAPER

View Article Online
View Journal | View Issue

Cite this: J. Mater. Chem. C, 2016, 4, 4459

Organic vapor sensing behaviors of conductive thermoplastic polyurethane–graphene nanocomposites†

Hu Liu,[ab] Wenju Huang,[a] Xinru Yang,[a] Kun Dai,*[a] Guoqiang Zheng,[a] Chuntai Liu,[a] Changyu Shen,[a] Xingru Yan,[b] Jiang Guo[b] and Zhanhu Guo*[b]

Received 8th March 2016,
Accepted 29th March 2016

DOI: 10.1039/c6tc00987e

www.rsc.org/MaterialsC

Conductive thermoplastic polyurethane (TPU) nanocomposites filled with graphene were fabricated and tested for organic vapor sensing. The observed finely dispersed graphene in the TPU matrix benefited from the formation of efficient conductive paths and the generation of stable electrical signals. Organic vapor sensing behaviors of the conductive polymer composites (CPCs) were evaluated using four kinds of organic vapors possessing different polarities (p), including cyclohexane (p = 0.1), tetrachloromethane (CCl_4, p = 1.6), ethylacetate (p = 4.3) and acetone (p = 5.4). Unlike conventional CPCs that only respond to certain specific groups of organic vapors, the current CPCs showed a novel negative vapor coefficient (NVC) effect for all tested vapors. This observed NVC was due to both the inherent microphase segregation structure of TPU containing soft and hard segments and the wrinkled structure of graphene. In successive immersion-drying runs (IDRs) at 30 °C, fast response, good reversibility and reproducibility were observed for the non- and low- polar vapors (cyclohexane and CCl_4), but residual resistance was observed for polar organic vapors (ethylacetate and acetone) after their desorption. The temperature dependent vapor sensing behaviors indicated that the vapor sensing responsivity increased with increasing the temperature due to higher absorption activation energy at higher temperature. This study provides guidelines for the fabrication of organic vapor sensors using CPCs possessing fast response, good discrimination ability and reproducibility.

1 Introduction

Recently, conductive polymer composites (CPCs) have been used in different sensors including strain,[1–3] temperature,[4–6] piezoresistance,[7,8] and vapor[9–14] arising from their excellent features, including ease of processing, low cost of fabrication and diversity of polymer candidates.[15] CPCs are normally achieved by dispersing one or more electrically conductive fillers into the insulating polymeric matrix and the interconnections of electrical conductive fillers build the conducting networks. The working principle of a 'smart sensor' is based on the sudden change in electrical resistance as a result of the re-arrangement of conductive paths when exposed to external stimuli.[16] As for CPC-based organic vapor sensors, the response mechanism is generally explained by the so-called electrical percolation theory.[17] The adsorption of organic vapors induces the swelling of the polymer matrix, causing the resistance variation resulting from the rearrangement of conductive paths. After the desorption of organic vapors, the conductive paths would fully or partially recover their initial states.

For most CPC-based organic vapor sensors, an increase of resistance would be observed when exposed to organic vapors, illustrating a positive vapor coefficient (PVC). For example, carbon nanotube (CNT)/polymethylmethacrylate[18] and CNT/poly(lactic acid)[19] nanocomposites displayed PVC sensing behavior towards organic vapors due to the increase in the distance between the adjacent conductive fillers. The increased distance was caused by the swelling of the polymer matrix. In addition, a negative vapor coefficient (NVC, the resistance of CPCs decreases when exposed to organic vapors) was also observed when the conductive filler loading was below the percolation threshold. For example, carbon black (CB)/water-borne polyurethane (WPU) composites with CB content below the percolation threshold displayed the NVC phenomenon.[20] Chen *et al.* suggested that the absorption of organic vapors damaged the hydrogen bonds between CB and PU, causing the

[a] School of Materials Science and Engineering, The Key Laboratory of Material Processing and Mold of Ministry of Education, Zhengzhou University, Zhengzhou, Henan 450001, China. E-mail: kundai@zzu.edu.cn
[b] Integrated Composites Laboratory (ICL), Department of Chemical & Biomolecular Engineering, University of Tennessee, Knoxville, TN 37996, USA. E-mail: zguo10@utk.edu

† Electronic supplementary information (ESI) available. See DOI: 10.1039/c6tc00987e

aggregation of CB particles and the decreased resistance. The appearance of a NVC significantly enhanced the discriminating ability of CPCs used as organic vapor sensors. However, an imperfect conductive network was formed when the conductive filler loading was below the percolation threshold, causing an unstable signal output. Herein, CPC-based organic vapor sensors with stable NVC out-put signals are essential for practical applications.

Generally, the ideal CPC-based organic vapor sensing materials require the properties of a high electrical conductivity, a wide test scope, good sensitivity and reproducibility. Nevertheless, there are two main problems in practice. First, a high electrical conductivity, which is essential for obtaining stable electrical signals, usually needs a large amount of conductive fillers to construct effective conductive paths, leading to the sacrifice of mechanical properties and increased production cost.[21,22] Second, due to the specific interaction between the polymer matrix and organic vapor, some conventional CPCs showed response only to certain groups of organic vapors and thus showed poor discriminating ability.[23,24] For example, Zhang *et al.* studied the vapor sensing behavior of carbon nanofiber/CB/polystyrene composites. They displayed good PVC sensing behaviors only towards the organic vapors that have analogous polarities to the polymer matrix.[24] Therefore, it is necessary to solve these problems to acquire high-performance gas sensors.

Graphene, a single layer of carbon atoms with a two dimensional structure, has been an attractive material for the fabrication of gas/vapor sensors due to its remarkable properties such as a large sensing area, high electrical conductivity and low inherent electrical noise.[25–27] On one hand, graphene could reduce the percolation threshold of CPCs effectively due to its good electrical conductivity and large aspect ratio. For instance, Liu *et al.* fabricated the graphene/thermoplastic polyurethane (TPU) nanocomposites and an ultralow percolation threshold of 0.1 wt% was reported.[3] The mechanical properties of the CPCs were also significantly enhanced. On the other hand, graphene-based gas/vapor sensors, including functionalized graphene decorated with nanocrystals or metal nanoparticles, showed tremendous advantages in gas sensing applications.[28–34] For example, Tung *et al.* prepared Ag-reduced graphene oxide (rGO) hybrid materials to develop organic vapor sensors. The Ag nanoparticles acted as spacers to separate graphene sheets, allowing more organic vapors to be absorbed on the large surface area of graphene, and thus rapid and reliable PVC response was obtained.[30]

TPU, a kind of elastomeric segmented copolymer, is composed of polar hard segments and nonpolar soft segments. Due to the polarity difference and crystallization, the hard segments can easily come together and scatter in the continuous phase of soft segments to form a 'micro-phase separation structure'.[35] According to 'like dissolves like' theory, unlike conventional CPC-based vapor sensors that respond only to certain specific groups of solvent vapors,[16,36] the soft segments and hard segments of TPU would be swollen by non-polar/low polar vapors and polar vapors separately, which would lead to the redistribution of conductive fillers in the polymer matrix and hence a unique resistance variation, showing its discriminating ability for different organic vapors. For example, Chen *et al.* synthesized CB/WPU composites for organic vapor sensing, showing sensitivity for organic vapors with various polarities due to the coexistence of non-polar and polar segments on polyurethane chains.[20] In spite of the aforementioned merits of both graphene and TPU, graphene/TPU nanocomposites with great potential as high-performance organic vapor sensors have not been reported yet.

In this study, TPU-based CPCs filled with different loading levels of graphene were fabricated. The dispersion states of graphene and the morphology of the CPCs were investigated using a transmission electron microscope (TEM) and a field emission scanning electron microscope (FE-SEM). The thermal stability of CPCs was tested by thermal gravimetric analysis (TGA). Their rheological behaviors were also studied. The feasibility of organic vapor sensors was evaluated using four kinds of organic vapors possessing different polarities (p), including cyclohexane (p = 0.1), tetrachloromethane (CCl_4, p = 1.6), ethylacetate (p = 4.3) and acetone (p = 5.4). The effect of temperature on the vapor sensing behaviors was disclosed. In addition, successive immersion-drying runs were applied to investigate their reproducibility.

2 Experimental

2.1 Materials and chemicals

TPU (BASF Elastollan 1185A, ρ = 1.12 g cm^{-3}) was bought from BASF Co. Ltd. An aqueous suspension with 0.45 wt% graphene (thickness: ~0.55–3.74 nm, diameter: ~0.5–3 μm) was purchased from Chengdu Organic Chemicals Co. Ltd, China. Dimethylformamide (DMF), methanol, cyclohexane, CCl_4, ethylacetate and acetone were supplied by Zhiyuan Reagent Co., Ltd, Tianjin, China. All the chemicals were used as received without any further treatment.

2.2 Fabrication of TPU-based CPCs

The brief procedures for fabricating the TPU-based CPCs are as follows. The TPU/DMF solutions were prepared by magnetic stirring at 40 °C (the polymer loading was fixed at 5 wt%) until TPU was completely dissolved. The graphene aqueous solution was added into DMF and sonicated (285 W) for 10 min to pre-disperse graphene; the dispersion was then added to the TPU/DMF solution (0.2, 0.4, 0.6 and 0.8 wt% with regard to the weight of graphene and TPU) and sonicated for 30 min. The blend was then transferred to methanol to immobilize the graphene in the TPU matrix and the CPCs were precipitated quickly from methanol. After that, the obtained CPCs were filtered, dried at 80 °C under vacuum for 20 h, and hot pressed at 210 °C for 10 min under a pressure of 15 MPa. The thickness of the obtained CPCs sample was controlled at 0.4 mm. Pure TPU was also prepared following the same procedures without adding graphene for comparison.

2.3 Characterization

Atomic-force microscopy (AFM) measurements were conducted in non-tapping mode using the VEECO Nanoscope IV instrument.

The sample was prepared by spin-coating the dilute graphene/DMF solution onto freshly cleaved mica substrates at 1000 rpm and drying in a vacuum oven. Transmission electron microscopy (TEM) imaging was performed using a JEOL JEM-1230 instrument at an acceleration voltage of 90 kV. The graphene sample was prepared by drying one droplet of dilute graphene/DMF solution on a holey carbon-coated copper TEM grid. The CPC sample was prepared by mixing the specimen with epoxy resin and cured at 70 °C for 24 h in a vacuum. Ultra-thin sections (~100 nm) were prepared using a Leica UC-7 ultramicrotome with a diamond knife at −90 °C. FE-SEM imaging was performed using a JEOL JSM-7500F instrument. The specimen was immersed in liquid nitrogen for an hour and broken quickly, and then the freeze-fractured surfaces were sputter-coated with a layer of platinum to prevent charging for improved imaging quality.

Thermogravimetric analysis (TGA) was carried out on a TGA/STDA851e (Mettler Toledo, Switzerland) from ambient temperature to 700 °C at a heating rate of 10 °C min^{-1} in a nitrogen atmosphere. The nitrogen flow rate was 40 mL min^{-1}. About 8 mg of the sample was used for each test.

The rheological behaviors of pure TPU and TPU-based CPCs were studied using a rheometer (AR1500ex, TA instrument). An environmental test chamber (ETC) steel parallel-plate geometry with a diameter of 25 mm was used to carry out the measurements. Dynamic oscillation frequency was swept from 100 to 0.1 Hz at a strain of 1% within the linear viscoelastic (LVE) range at 200 °C under an air atmosphere. The diameter of the samples used for this test was 25 mm with ~2 mm thickness.

The organic vapor discriminating ability of the CPCs was evaluated by recording their resistance variation towards four typical organic solvent vapors with different polarities (p), including cyclohexane (p = 0.1), CCl_4 (p = 1.6), ethylacetate (p = 4.3) and acetone (p = 5.4). In order to study the vapor sensing reproducibility of the CPCs, five successive immersion-drying runs (IDRs) of the samples against each organic vapor were performed. For an IDR, after achieving a stable baseline in air for 50 s, the sample was immersed in a saturated organic vapor for a period of 100 s and then dried in air for 150 s. In order to study the temperature dependence of the organic vapor sensing behaviors, the IDRs were also conducted at different temperatures, including 30, 35, 40, 45 and 50 °C. The resistances of the CPCs were recorded online by using a precision digital resistor (Model TH2683, Changzhou Tonghui Electronics Co. Ltd, China) at a constant voltage of 10 V. The corresponding responsivity was calculated by the relative resistance $((R - R_0)/R_0 \times 100\%$, where R represents the transient resistance during the IDR and R_0 is the resistance of the sample after stabilization in air).

3. Results and discussion

3.1 Morphological observations

Fig. 1 shows the morphologies of graphene and the cross-section of CPCs. Graphene with lateral dimensions of about 1 μm and a thickness of about 1.05 nm was obtained after sonication dispersion, showing a nearly monolayer dispersion, Fig. 1a and b.[37–39] The flake-like morphology of the freeze-fractured surface of CPCs was observed, Fig. 1c. The graphene sheets were wrapped well by the TPU matrix, showing a good interface adhesion between graphene and the polymer matrix. In the TEM image (Fig. 1d), graphene with wrinkled structure was finely dispersed throughout the TPU matrix, and the nanosheets contact each other, providing efficient conductive pathways for electron transport.[40]

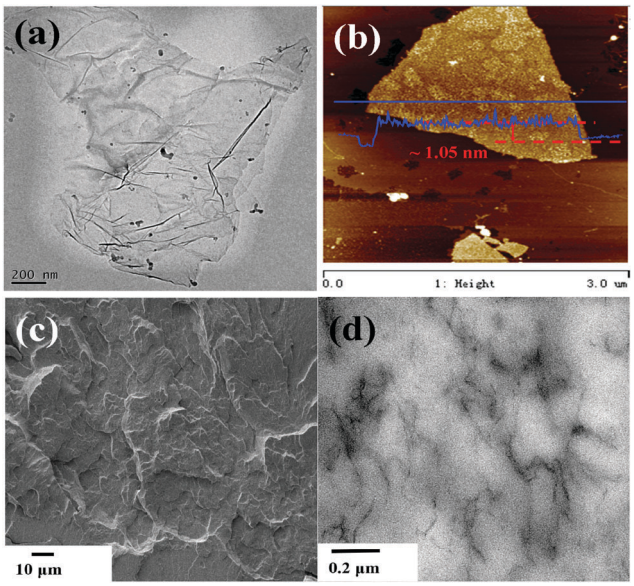

Fig. 1 Typical (a) TEM image and (b) the non tapping-mode AFM image of graphene dispersed in DMF; (c) the FE-SEM image of the freeze-fractured surface and (d) the TEM image of CPCs containing 0.4 wt% graphene.

3.2 Rheological measurements

The rheological behaviors of pure TPU and its CPCs at 200 °C were studied to obtain information about graphene conductive networks depending on the filler–matrix interactions. Fig. 2a and b depict the storage modulus (G') and loss modulus (G'') as a function of oscillation frequency (Hz). A monotonic increase of G' in all the frequency range was observed for pure TPU and its CPCs. With the increase of graphene loading, the G' shows a larger enhancement at lower frequency than that at higher frequency. The reason may be related to the interactions between graphene and the TPU matrix, which restrain the mobility of polymer chains.[41] In addition, a plateau corresponding to a liquid-to-solid transition[42] was also found in a lower frequency range (0.1–1 Hz), and was attributed to the formation of graphene conductive networks in the TPU matrix and the strong interaction between the two components.[43,44] The curves of G'' exhibit a similar trend to G', but the enhancement of G'' appears in a narrower range (0.1–0.4 Hz) and an inconspicuous plateau is observed for the CPCs with a graphene loading of 0.8 wt%. This indicates that the energy dissipation effect is not significantly influenced by the addition of the graphene filler.

The complex viscosity (η^*) as a function of oscillation frequency was also studied, Fig. 2c. For both pure TPU and its

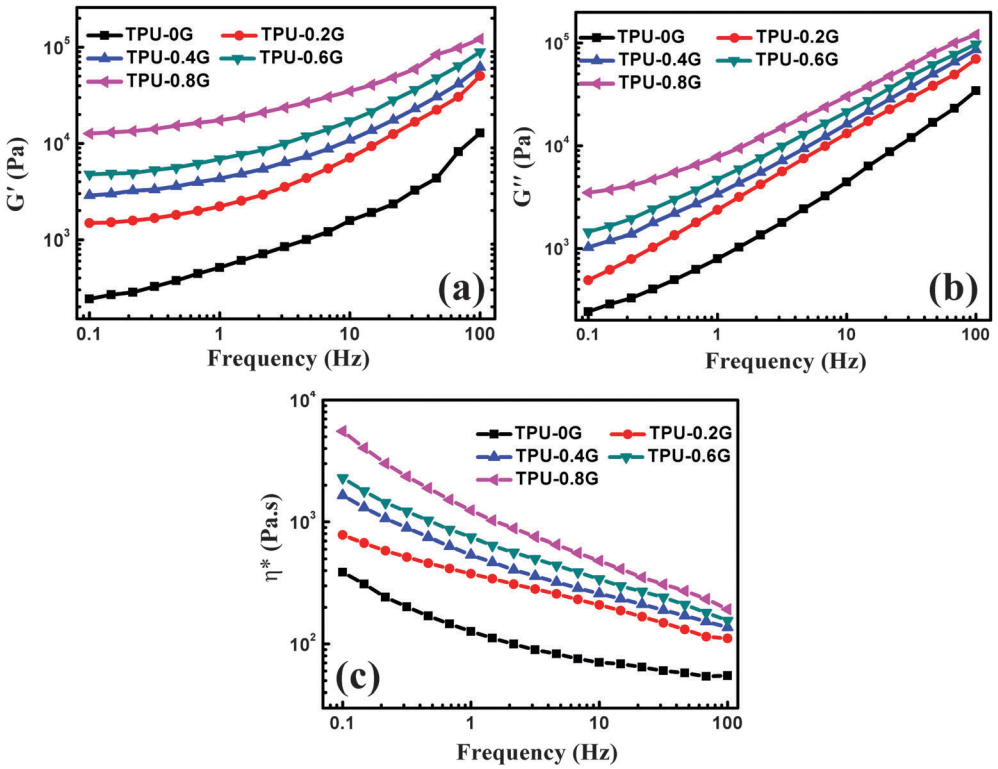

Fig. 2 Rheological behaviors of pure TPU and its CPCs containing different graphene loading levels by (a) storage modulus, (b) loss modulus and (c) complex viscosity *versus* frequency at 200 °C.

CPCs, the η^* decreased monotonically with increasing oscillation frequency in all the frequency ranges, showing a typical shear thinning phenomenon.[45,46] The η^* increased with increasing the graphene loading in all the frequency ranges, especially in the lower frequency range of 0.1–1 Hz. This suggests that the mobility of TPU marcomolecular chains was restrained by the addition of graphene, causing a higher viscosity.

3.3 Thermogravimetric analysis

Fig. 3 shows TGA and the corresponding differential thermogravimetric analysis (DTG) curves of pure TPU and its CPCs in a nitrogen atmosphere. Here, $T_{5\%}$ (the temperature for 5% weight loss) is defined as the onset decomposition temperature and T_p is defined as the temperature of the maximum decomposition rate. The inset of Fig. 3a is an enlarged plot around 5% weight loss. The onset decomposition temperature of the CPCs is observed to increase with increasing the graphene loading, and it reaches 311.2 °C at 0.4 wt% graphene loading, which is 5.8 °C higher than that for neat TPU. However, the thermal stability shows a reducing trend for the CPCs containing 0.6 and 0.8 wt% graphene. Similar results were also observed for graphene/linear low density polyethylene (LLDPE) composites.[47] In addition, as shown in Fig. 3b, both neat TPU and its CPCs are decomposed in a two-step process. The first step at about 342 °C is attributed to the cleavage of urethane bonds. At this temperature, the decomposition peak becomes weaker

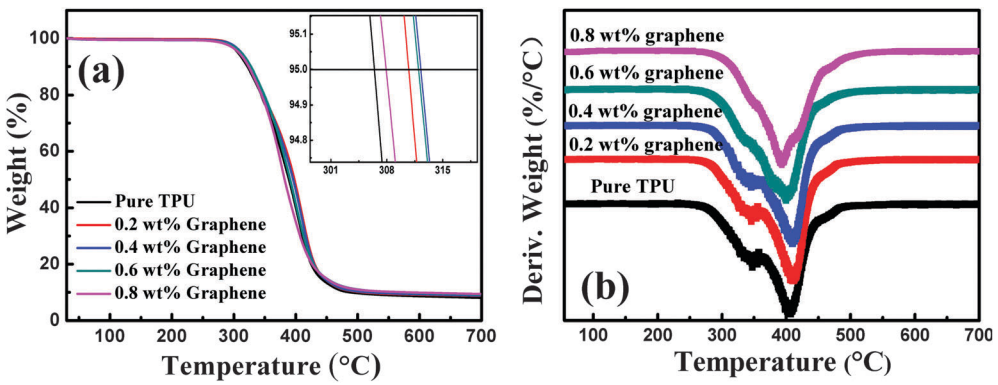

Fig. 3 (a) TGA and (b) DTG curves of pure TPU and its CPCs containing different graphene loading levels.

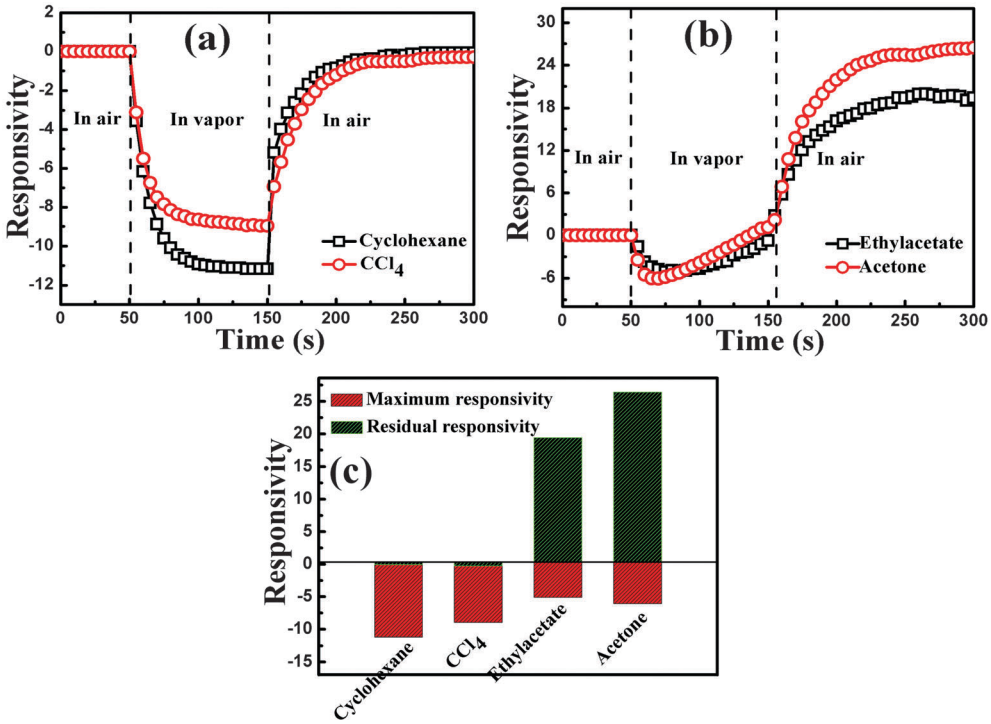

Fig. 4 Responsivity of TPU-based CPCs containing 0.4 wt% graphene towards saturated (a) cyclohexane & CCl_4 and (b) ethylacetate & acetone as a function of time; (c) the maximum responsivity in saturated organic vapors and the residual responsivity in air in a single IDR at 30 °C.

gradually and it almost disappears when the graphene loading is increased to 0.8 wt%. For the second step of the decomposition of soft segments, the T_p of the CPCs with different graphene loadings has a similar trend to $T_{5\%}$. The CPCs containing 0.2 wt% graphene possess the highest T_p (410.5 °C, 6.6 °C higher than neat TPU).

All of the results indicate that the thermal stability was slightly improved even with a low graphene loading. The improvement is attributed to the homogeneously distributed graphene, which acts as a so-called 'tortuous path' to slow down the diffusion of volatile decomposition products and retard the release of these products.[48,49] As for the reduced thermal stability of CPCs at higher graphene loadings, it might be due to excellent thermal stability and thermal conductivity of graphene, which acts as a heat source to induce thermal decomposition at a higher loading.[47] In addition, a higher graphene loading also damages the 'micro-phase separation structure', resulting in a reduced thermal stability.

3.4 Organic vapor sensing behavior

An ultra-low percolation threshold ($P_c \sim 0.1$ wt%) is reported to be achieved for graphene/TPU nanocomposites.[3] A CPC-based organic vapor sensor should have a stable output signal, and thus CPCs containing 0.4 wt% graphene, well above the percolation region, were used to examine the electrical resistance response against different organic vapors.

For the application of a favorable vapor sensor, the vapor discriminating ability and quick response are key features.[19] In this paper, the sensing selectivity of these TPU-based CPCs was evaluated towards a set of organic vapors with different polarities, including cyclohexane (0.1), CCl_4 (1.6), ethylacetate (4.3) and acetone (5.4). The responsivity of CPCs was recorded continuously, Fig. 4. CPCs are observed to exhibit different sensing behaviors against different organic vapors, indicating that they are good candidates for vapor sensors with good discriminating ability. For non-/low-polar organic vapors (cyclohexane and CCl_4), the CPCs' resistance encounters a sharp decrease and reaches an equilibrium when exposed to organic vapors, showing the NVC phenomenon.[36,50] When they were exposed to air, the resistance increases sharply and almost returns to its initial value, showing a fast response rate and good reversibility. As for polar organic vapors (ethylacetate and acetone), the resistance decreases to a minimum value at first and then increases gradually when exposed to organic vapors. When they were exposed to air, interestingly, it continues to increase and reaches a higher value eventually than the initial one. This indicates that an obvious residual resistance is obtained after the desorption of organic vapors. All responsivities (defined as $(R_t - R_0)/R_0$, where R_0 denotes the initial resistance of the CPCs and R_t denotes the resistance at time t during the test) of the CPC-based sensors towards organic vapors with different polarities are shown in Fig. 4c. For organic vapors, the ranking of maximum responsivity is as follows: cyclohexane (−11.2) > CCl_4 (−8.96) > acetone (−6.06) > ethylacetate (−5.11). The corresponding maximum responsivity towards each vapor is an important parameter to detect and specify due to different interactions between the organic vapor and the

polymer matrix. For air, the ranking of residual responsivity is: acetone > ethylacetate > CCl_4 ≈ cyclohexane. The abundant variations of vapor sensing behaviors can be attributed to the evolution of conductive paths distributed in the TPU matrix, which is induced by the interactions between the organic vapor and the TPU matrix. For vapor sensing, when the CPCs were immersed in the organic vapors, the absorption of organic vapors led to the swelling of the polymer matrix, causing the change in conductive paths. In the drying process, the organic vapor molecules would desorb from the polymer matrix, and all or partial conductive paths would return to their initial states. The organic vapor sensing behaviors of several other CPCs have been compared, and graphene/TPU CPCs show a stable NVC behavior at such a low graphene loading, which significantly enhances their discriminating ability and enables them to be used as organic vapor sensors (Table S1, ESI†).

The corresponding mechanism of the interactions between the organic vapor and the TPU matrix can be explained as follows. As mentioned above, TPU is composed of non-polar soft segments and polar hard segments, and has an interesting microphase segregation structure. According to the rule of 'like dissolves like',[51] the non-/low-polar vapors (cyclohexane and CCl_4) mainly interact with the non-polar soft segments of TPU and result in the swelling of the soft segment rich microphase. Due to the winding structure of soft segments and the large aspect ratio and the wrinkled structure of graphene, the swelling would rearrange the macromolecular chain structure and lead to more overlapping between graphene sheets, causing a more perfect conductive network and a decreased resistance. This interesting phenomenon has rarely been reported in the literature to the best of our knowledge. On the other hand, cyclohexane possesses a little lower polarity than CCl_4, and thus it has a stronger interaction with soft segments than CCl_4, and a higher vapor sensing responsivity is thus obtained. In the drying process, the vapor molecules desorb from the polymer matrix and the non-polar soft segments contract gradually due to their good elasticity, and the conductive networks thus return to their initial state.

Polar organic vapors (ethylacetate and acetone) mainly interact with polar hard segments of the TPU matrix, which would swell during the immersion process. Owing to the fact that the hard segments act as physical crosslinkers in the TPU matrix, the swelling of hard segments would lead to the release of soft segments, causing partial rearrangement of the conductive paths in the soft segments.[35] Therefore, a quick decrease of resistance occurs in the initial stage, Fig. 4b. However, compared to the rearrangement of conductive paths in the soft segments, the swelling of the rigid hard segments, which leads to the destruction of the conductive network and the increase of tunneling resistance, still plays a leading role, and thus the resistance is increased again. The hard segments cannot return to their initial state during the vapor evaporation process due to the poor mobility of macromolecular chains in this microphase, causing the permanent destruction of conductive pathways. A residual resistance is observed after the desorption of organic vapors. Besides, the higher polarity of acetone results in higher responsivity and residual resistance than ethylacetate vapor.

Generally, for CB[9,52] or CNT[19,53] filled CPC-based liquid/vapor sensors with a conductive filler content above the percolation threshold, positive vapor coefficient (PVC) phenomena were observed when immersed in an organic solvent/vapor. It is widely accepted that the conductive network consisting of rod-like CNTs or spherical CB is easier to be destroyed by the swelling of the polymer matrix, causing the increase of electrical resistance. Here, thanks to the microphase segregation structure of TPU and the wrinkled structure of graphene, the CPCs exhibit a novel negative vapor coefficient (NVC) phenomenon, enhancing their discriminating ability.

The responsivity of CPCs towards organic vapors in five successive IDRs at 30 °C was investigated to evaluate their stability and reproducibility (Fig. 5). Towards the vapors of cyclohexane and CCl_4, the CPCs show a similar sensing behavior pattern and the resistance almost returns to the initial value after being exposed to air in each IDR, showing good vapor reversibility and reproducibility. Additionally, the electrical signals are stable and the sensing behaviors exhibit a quick response rate, which is an important advantage compared to metal oxide-based vapor sensors.[54] For sensing behaviors of CPCs toward the vapors of ethylacetate and acetone, the resistance response curve increases slightly in the following cycles, which is also observed for the CB/poly(lactic acid) and CNT/poly(lactic acid)

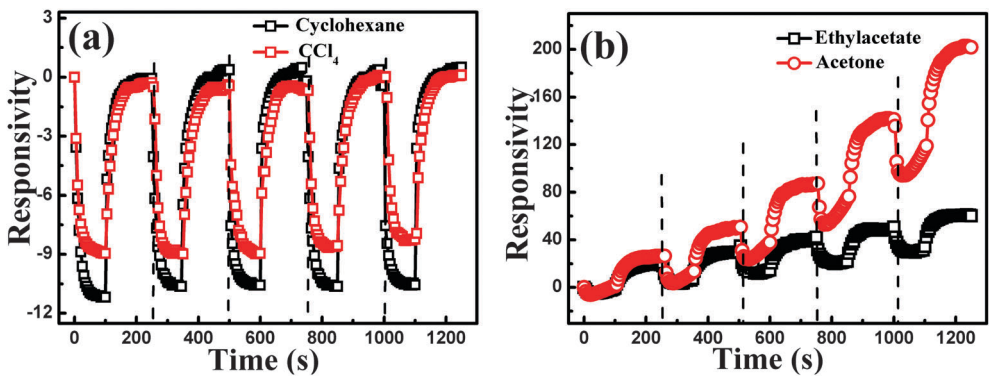

Fig. 5 Responsivity of TPU-based CPCs containing 0.4 wt% graphene towards saturated (a) cyclohexane & CCl_4 and (b) ethylacetate & acetone vapors in five IDRs at 30 °C.

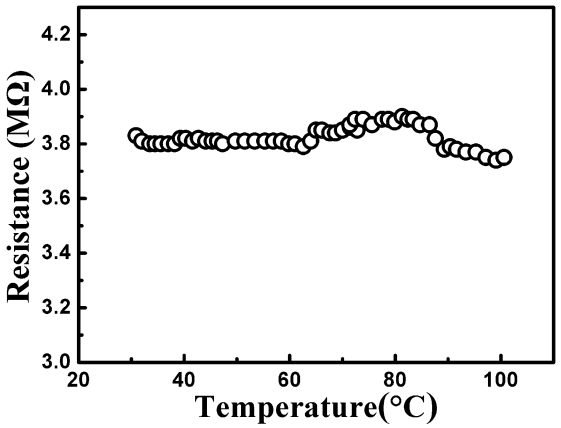

Fig. 6 Temperature dependent resistance of TPU-based CPCs containing 0.4 wt% graphene.

nanocomposites due to the permanent destruction of conductive paths.[55] All the aforementioned results indicate that the CPCs have great potential to detect organic vapors with different polarities.

3.5 Temperature dependence of organic vapor sensing behavior

Generally, environmental temperature affects the vapor sensing performance owing to the joint influences of the thermal field and the vapor pressure.[56] A positive or negative temperature coefficient is often observed for CPC systems, such as CB/polyamide-6/high density polyethylene,[4] carbon fiber/ultra-high molecular weight polyethylene/polyvinylidene fluoride[57] and CB/polypropylene/ultra-high density polyethylene,[58] due to the volume expansion of the polymer matrix with increasing the temperature, which subsequently causes the damage of conductive paths. The temperature dependence of the resistance of CPCs in air was measured from room temperature to 100 °C to understand the thermal stability of CPCs. As shown in Fig. 6, the resistance exhibits a slight fluctuation throughout the whole temperature range, which is due to the low crystallinity of the TPU matrix, which generates traces of volume expansion during the heating process. Thus, it is deduced that the thermal induced resistance variation has a negligible impact on the temperature dependence of vapor sensing behavior.

Fig. 7 illustrates the organic vapor sensing responsivity of CPCs towards different organic vapors at different temperatures. During exposure to organic vapors, the maximum responsivity of CPCs increases with increasing the temperature for all tested organic vapors (Fig. S1a, ESI†). After the desorption of organic vapors in air, the residual resistance of CPCs remarkably increases towards the vapors of ethylacetate and acetone with increasing temperature. There is almost no change for the vapors of cyclohexane and CCl_4 (Fig. S1b, ESI†). These phenomena can be explained as follows. The increase of the testing temperature leads to a higher saturated vapor pressure, the vapor adsorption is thus accelerated, causing more serious swelling due to the interaction between organic vapor and TPU macromolecular

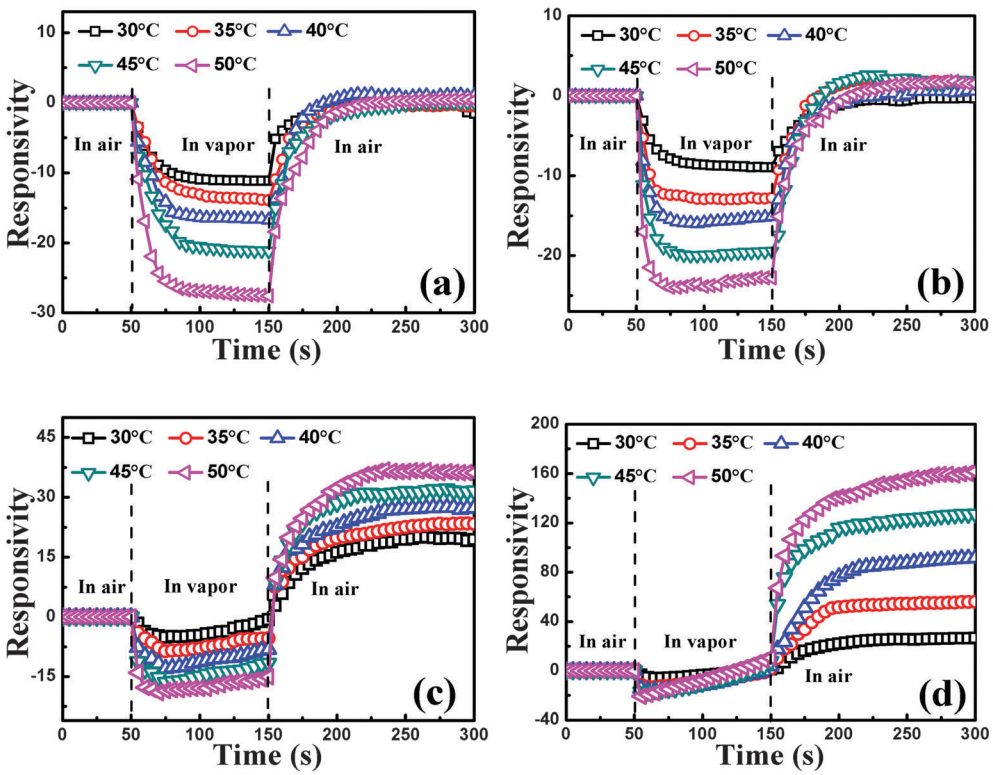

Fig. 7 Responsivity of TPU-based CPCs containing 0.4 wt% graphene towards saturated (a) cyclohexane, (b) CCl_4, (c) ethylacetate and (d) acetone vapors in a single IDR at different temperatures.

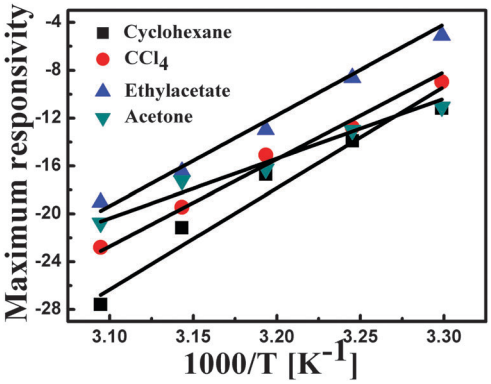

Fig. 8 Maximum responsivity magnitude of TPU-based CPCs containing 0.4 wt% graphene in different saturated vapors as a function of inverse temperature (1/*T*).

chains, the conductive paths are thus affected more obviously than the samples tested at a lower temperature.[53] As mentioned above, the larger maximum responsivity is caused by the greater degree of soft segments' expansion or the release from hard segments at a higher temperature. As for the residual resistance, the soft segments shrink after the desorption of cyclohexane and CCl_4 vapors, and almost no residual resistance is observed; the hard segments cannot return to their initial state completely, especially at a higher temperature, and a more severe permanent destruction of conductive paths occurs after the desorption of vapors of ethylacetate and acetone, showing a higher residual responsivity.

Here, the maximum responsivity magnitudes of CPCs towards different vapors as a function of inverse temperature were plotted to further reveal the effect of temperature (Fig. 8), and a good linear relationship was observed. This is naturally connected with the Arrhenius equation, which is used to describe the process of thermal activation. The slope represents the absorption activation energy of the corresponding vapor.[55] As discussed for the CB/PU[52] and CNT/PU[55] systems, the absorption rates of the composites increase with increasing the temperature, causing higher responsivity. Therefore, the Arrhenius-like dependence of maximum responsivity on the inverse temperature factually reflects the controlling mechanism of the electrical response behavior of the CPCs at different vapor temperatures.

Five successive IDRs of the TPU-based CPCs were also conducted to evaluate its stability and reproducibility at different temperatures. Towards the cyclohexane vapor, the CPCs are observed to maintain good reproducibility on each loop at all the test temperatures (Fig. 9a). For the CCl_4 vapor, Fig. 9b, it exhibits good reversibility and reproducibility at 30 °C, but the response curve slightly shifts to a higher responsivity in the subsequent runs at higher temperatures; small residual responsivity is observed gradually. The results indicate that the low polar CCl_4 vapor turns out to be a better solvent for hard segments at high temperatures. For vapors of ethylacetate and acetone (Fig. 9c and d), the responsivities show tremendous enhancements with increasing temperature. Linear plots of the residual responsivity against temperature are also given in Fig. 10, and the slopes represent the extent of the interaction between the organic vapor and the hard segments of the TPU matrix.

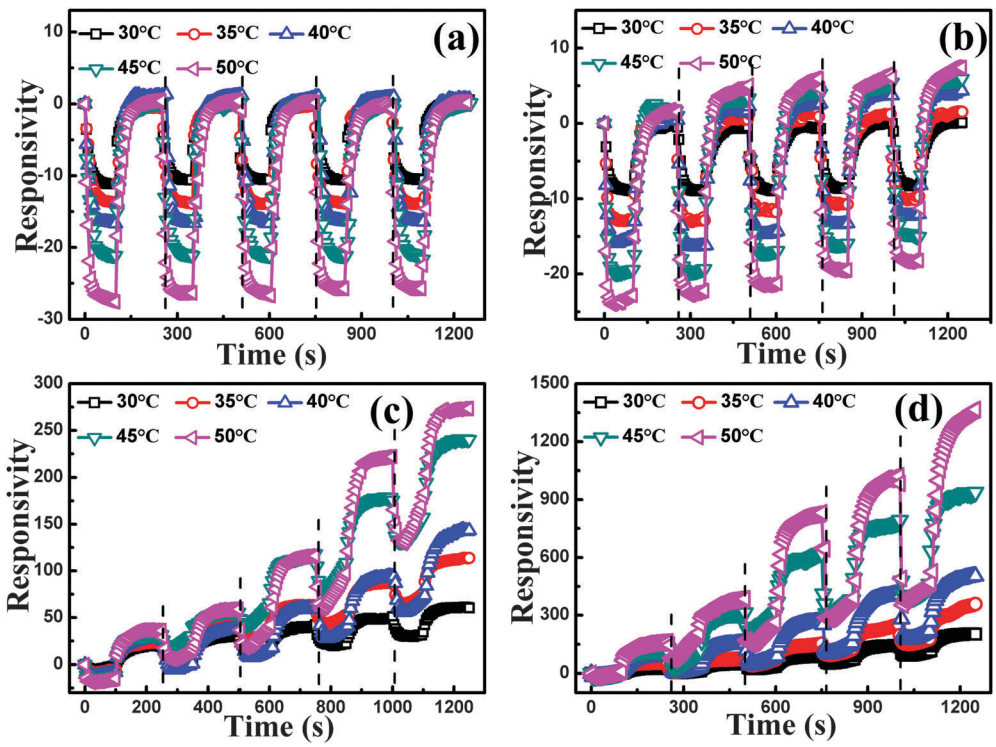

Fig. 9 Responsivity of TPU-based CPCs containing 0.4 wt% graphene towards saturated (a) cyclohexane, (b) CCl_4, (c) ethylacetate and (d) acetone vapors at different temperature in five IDRs.

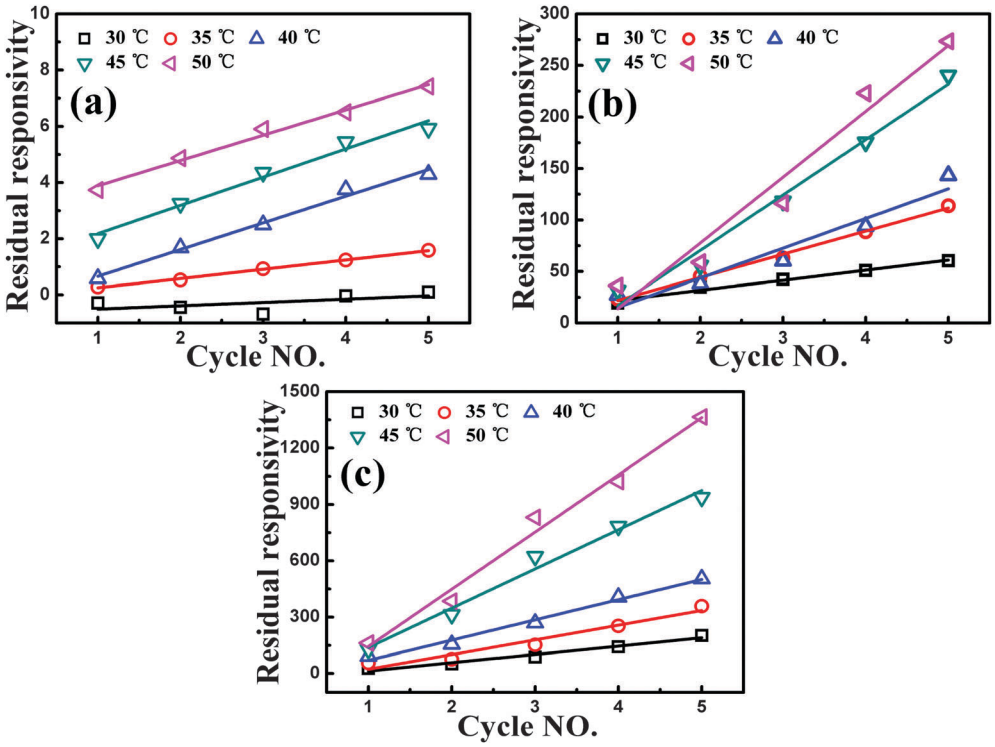

Fig. 10 Linear plots of the residual responsivity towards saturated (a) CCl_4, (b) ethylacetate and (c) acetone vapors against the cycle number at different temperatures.

A bigger slope is observed at higher temperature for each organic vapor, resulting in higher responsivity due to the stronger interaction. This phenomenon can be explained as follows. The larger quantity of absorbed organic vapor at higher temperature due to higher absorption activation energy caused the swelling of hard segments and the release of more soft segments, all these contributed to a higher responsivity. In addition, it is known that the Florry–Huggins interaction parameter,[56] which is used to evaluate the solvent–polymer matrix interaction, decreases with increasing temperature. A lower value indicates a higher solubility of the polymer in relevant solvents. Thus, the interaction becomes stronger with increasing the temperature. Due to the microphase segregation structure of TPU and the wrinkled structure of graphene, the CPCs exhibit different gas sensing behaviors against different organic vapors and temperatures, showing great potential for applications as organic vapor sensors.

4 Conclusions

The TPU-based CPCs filled with finely dispersed graphene were fabricated and tested for organic vapor detection. The storage modulus, loss modulus and complex viscosity were enhanced for all the CPCs at all graphene loadings, especially in the low frequency range of 0.1–1 Hz. A rheological plateau at low oscillation frequency was formed due to the formation of graphene conductive networks in the TPU matrix and a strong interaction between them. Organic vapor sensing behaviors towards four typical organic vapors (cyclohexane, CCl_4, ethylacetate and acetone) with different polarities were observed in successive IDRs. According to the rule of 'like dissolves like', the non-polar and low polar vapors (cyclohexane and CCl_4) caused the non-polar soft segments of TPU to swell, and the rearrangement of the winding soft segment macromolecules induced a more perfect conductive network. The CPCs' resistance shows a fast decrease, illustrating a NVC phenomenon. After the desorption of vapor molecules, the conductive network returns to its initial state due to good elasticity of soft segments, showing good reproducibility. However, the observed NVC phenomenon in the polar organic vapors (ethylacetate and acetone) is attributed to the released soft segments from the swollen hard segments. Meanwhile, the destruction cannot be fully recovered in the drying process due to the poor mobility of the macromolecular chain in hard segments, causing a residual resistance. The vapor sensing responsivity was observed to increase with increasing the temperature due to higher absorption activation energy at higher temperature. The non-polar soft segments and polar hard segments of TPU enabled it to interact with organic vapors with different polarities, leading to the corresponding vapor sensing behavior and maximum responsivity. In addition, the microphase separation structure of TPU and the wrinkled structure of graphene resulted in an interesting NVC phenomenon, which enhanced the discriminating ability of the CPCs as organic vapor sensors. This study provides guidelines for the fabrication of organic vapor sensors using conductive polymer composites possessing fast response, good discrimination ability and reproducibility.

Acknowledgements

The authors gratefully acknowledge the financial support of National Natural Science Foundation (Contract Number: 11572290, 11432003), China Postdoctoral Science Foundation (Contract Number: 2015M580637) and Special Science Foundation for Excellent Youth Scholars of Zhengzhou University (Contract Number 1421320041). Z. Guo appreciates the start – up fund from University of Tennessee Knoxville. H. Liu acknowledges the support from the China Scholarship Council.

References

1 J. Zhao, K. Dai, C. Liu, G. Zheng, B. Wang, C. Liu, J. Chen and C. Shen, *Composites, Part A*, 2013, **48**, 129–136.
2 J. Zhu, S. Wei, J. Ryu and Z. Guo, *J. Phys. Chem. C*, 2011, **115**, 13215–13222.
3 H. Liu, Y. Li, K. Dai, G. Zheng, C. Liu, C. Shen, X. Yan, J. Guo and Z. Guo, *J. Mater. Chem. C*, 2016, **4**, 157–166.
4 Y. Qu, W. Zhang, K. Dai, G. Zheng, C. Liu, J. Chen and C. Shen, *Mater. Lett.*, 2014, **132**, 48–51.
5 M. Rahaman, T. K. Chaki and D. Khastgir, *J. Mater. Sci.*, 2013, **48**, 7466–7475.
6 Z.-M. Dang, W.-K. Li and H.-P. Xu, *J. Appl. Phys.*, 2009, **106**, 024913.
7 J. J. Ku-Herrera and F. Aviés, *Carbon*, 2012, **50**, 2592–2598.
8 H. Liu, W. Huang, J. Gao, K. Dai, G. Zheng, C. Liu, C. Shen, X. Yan, J. Guo and Z. Guo, *Appl. Phys. Lett.*, 2016, **108**, 011904.
9 K. Li, K. Dai, X. Xu, G. Zheng, C. Liu, J. Chen and C. Shen, *Colloid Polym. Sci.*, 2013, **291**, 2871–2878.
10 K. Dai, Y.-C. Zhang, J.-H. Tang, X. Ji and Z.-M. Li, *J. Appl. Polym. Sci.*, 2012, **124**, 4466–4474.
11 L. Zhang, C. Li, A. Liu and G. Shi, *J. Mater. Chem.*, 2012, **22**, 8838–8843.
12 J. Chen and N. Tsubokawa, *Polym. Adv. Technol.*, 2000, **11**, 101–107.
13 P. Slobodian, P. Riha, A. Lengalova, P. Svoboda and P. Saha, *Carbon*, 2011, **49**, 2499–2507.
14 B. Zhang, X. Dong, R. Fu, B. Zhao and M. Zhang, *Compos. Sci. Technol.*, 2008, **68**, 1357–1362.
15 G. A. Sotzing, S. M. Briglin, R. H. Grubbs and N. S. Lewis, *Anal. Chem.*, 2000, **72**, 3181–3190.
16 J. R. Li, J. R. Xu, M. Q. Zhang and M. Z. Rong, *Macromol. Mater. Eng.*, 2003, **288**, 103–107.
17 X. M. Dong, R. W. Fu, M. Q. Zhang, B. Zhang, J. R. Li and M. Z. Rong, *Carbon*, 2003, **41**, 371–374.
18 B. Philip, J. K. Abraham, A. Chandrasekhar and V. K. Varadan, *Smart Mater. Struct.*, 2003, **12**, 935–939.
19 B. Kumar, M. Castro and J. F. Feller, *Sens. Actuators, B*, 2012, **161**, 621–628.
20 S. G. Chen, J. W. Hu, M. Q. Zhang, M. W. Li and M. Z. Rong, *Carbon*, 2004, **42**, 645–651.
21 J.-F. Gao, Z.-M. Li, Q.-J. Meng and Q. Yang, *Mater. Lett.*, 2008, **62**, 3530–3532.
22 H. Pang, D.-X. Yan, Y. Bao, J.-B. Chen, C. Chen and Z.-M. Li, *J. Mater. Chem.*, 2012, **22**, 23568–23575.
23 M. Castro, J. Lu, S. Bruzaud, B. Kumar and J.-F. Feller, *Carbon*, 2009, **47**, 1930–1942.
24 B. Zhang, R. Fu, M. Zhang, X. Dong, B. Zhao, L. Wang and C. U. Pittman Jr., *Composites, Part A*, 2006, **37**, 1884–1889.
25 A. K. Geim, *Science*, 2009, **324**, 1530–1534.
26 W. Yuan and G. Shi, *J. Mater. Chem. A*, 2013, **1**, 10078–10091.
27 C. Soldano, A. Mahmood and E. Dujardin, *Carbon*, 2010, **48**, 2127–2150.
28 J. L. Johnson, A. Behnam, S. J. Pearton and A. Ural, *Adv. Mater.*, 2010, **22**, 4877–4880.
29 W. Yuan, A. Liu, L. Huang, C. Li and G. Shi, *Adv. Mater.*, 2013, **25**, 766–771.
30 T. T. Tung, M. Castro, T. Y. Kim, K. S. Suh and J. F. Feller, *Anal. Bioanal. Chem.*, 2014, **406**, 3995–4004.
31 L. Zhou, F. Shen, X. Tian, D. Wang, T. Zhang and W. Chen, *Nanoscale*, 2013, **5**, 1564–1569.
32 Q. Ji, I. Honma, S.-M. Paek, M. Akada, J. P. Hill, A. Vinu and K. Ariga, *Angew. Chem., Int. Ed.*, 2010, **49**, 9737–9739.
33 L. Al-Mashat, K. Shin, K. Kalantar-zadeh, J. D. Plessis, S. H. Han, R. W. Kojima, R. B. Kaner, D. Li, X. Gou, S. J. Ippolito and W. Wlodarski, *J. Phys. Chem. C*, 2010, **114**, 16168–16173.
34 Z. Wu, X. Chen, S. Zhu, Z. Zhou, Y. Yao, W. Quan and B. Liu, *Sens. Actuators, B*, 2013, **178**, 485–493.
35 E. Segal, R. Tchoudakov, M. Narkis and A. Siegmann, *Polym. Eng. Sci.*, 2002, **42**, 2430–2439.
36 J. R. Li, J. R. Xu, M. Q. Zhang and M. Z. Rong, *Carbon*, 2003, **41**, 2353–2360.
37 S. Stankovich, D. A. Dikin, G. H. B. Dommett, K. M. Kohlhaas, E. J. Zimney, E. A. Stach, R. D. Piner, S. T. Nguyen and R. S. Ruoff, *Nature*, 2006, **442**, 282–286.
38 S. Stankovich, R. D. Piner, X. Chen, N. Wu, S. T. Nguyen and R. S. Ruoff, *J. Mater. Chem.*, 2006, **16**, 155–158.
39 W. Yuan, A. Liu, L. Huang, C. Liu and G. Shi, *Adv. Mater.*, 2012, **25**, 766–771.
40 D. A. Nguyen, Y. R. Lee, A. V. Raghu, H. M. Jeong, C. M. Shin and B. K. Kim, *Polym. Int.*, 2009, **58**, 412–417.
41 X. Yan, Q. He, X. Zhang, H. Gu, H. Chen, Q. Wang, L. Sun, S. Wei and Z. Guo, *Macromol. Mater. Eng.*, 2014, **299**, 485–494.
42 T. Chatterjee and R. Krishnamoorti, *Soft Matter*, 2013, **9**, 9515–9529.
43 J. Zhu, S. Wei, Y. Li, L. Sun, N. Haldolaarachchige, D. P. Young, C. Southworth, A. Khasanov, Z. Luo and Z. Guo, *Macromolecules*, 2011, **44**, 4382–4391.
44 Q. He, T. Yuan, J. Zhu, Z. Luo, N. Haldolaarachchige, L. Sun, A. Khasanov, Y. Li, D. P. Young, S. Wei and Z. Guo, *Polymer*, 2012, **53**, 3642–3652.
45 J. Kim, S. M. Hong, S. Kwak and Y. Seo, *Phys. Chem. Chem. Phys.*, 2009, **11**, 10851–10859.
46 P. M. Wood-Adams and J. M. Dealy, *Macromolecules*, 2000, **22**, 7489–7499.
47 T. Kuila, S. Bose, C. E. Hong, M. E. Uddin, P. Khanra, N. H. Kim and J. H. Lee, *Carbon*, 2011, **49**, 1033–1051.
48 X. Wang, Y. Hu, L. Song, H. Yang, W. Xing and H. Lu, *J. Mater. Chem.*, 2011, **21**, 4222–4227.
49 Y. Cao, J. Feng and P. Wu, *Carbon*, 2010, **48**, 3834–3839.
50 J. Chen and N. Tsubokawa, *Polym. J.*, 2000, **32**, 729–736.

51 S. G. Chen, X. L. Hu, J. Hu, J. Hu, M. Q. Zhang, M. Z. Rong and Q. Zheng, *Compos. Sci. Technol.*, 2006, **119**, 110–117.
52 K. Dai, S. Zhao, W. Zhai, G. Zheng, C. Liu, J. Chen and C. Shen, *Composites, Part A*, 2013, **55**, 11–18.
53 S. Shang, W. Zeng and X.-M. Tao, *Sens. Actuators, B*, 2012, **166–167**, 330–337.
54 F. Paraguay D., M. Miki-Yoshida, J. Morales, J. Solis and W. Estrada L., *Thin Solid Films*, 2000, **373**, 137–140.
55 S. G. Chen, J. W. Hu, M. Q. Zhang and M. Z. Rong, *Sens. Actuators, B*, 2005, **105**, 187–193.
56 Y. Li, H. Liu, K. Dai, G. Zheng, C. Liu, J. Chen and C. Shen, *Sens. Actuators, B*, 2015, **221**, 1279–1289.
57 J.-W. Zha, W.-K. Li, R.-J. Liao, J. Bai and Z.-M. Dang, *J. Mater. Chem. A*, 2013, **1**, 843–851.
58 Y. Wei, Z. Li, X. Liu, K. Dai, G. Zheng, C. Liu, J. Chen and C. Shen, *Colloid Polym. Sci.*, 2014, **292**, 2891–2898.